Bernstein - Bézier based finite elements for efficient solution of short wave problems

A. El Kacimi[1], O. Laghrouche[2], M.S. Mohamed[2], and J. Trevelyan[3]

[1]Laboratory of Modeling and Combinatorial, FP Safi, Cadi Ayyad University, Morocco
[2]Institute for Infrastructure and Environment, Heriot-Watt University, Edinburgh EH14 4AS, UK
[3]Department of Engineering, Durham University, Durham DH1 3LE, UK

Abstract

In this work, the Bernstein-Bézier Finite Element Method (BBFEM) is implemented to solve short wave problems governed by the Helmholtz equation on unstructured triangular mesh grids. As for the hierarchical Finite Element (FE) approach, this high order FE method benefits from the use of static condensation which is an efficient tool for reducing the total number of degrees of freedom and bandwidth of high order FE global matrices. The performance of BBFEM with static condensation (BBFEMs) is assessed via three benchmark problems and compared to that of the Partition of Unity Finite Element Method (PUFEM) in terms of accuracy, conditioning and memory requirement. Numerical results dealing with problems of Hankel sources interference and wave scattering by a rigid cylinder on quasi-uniform mesh grids indicate that BBFEMs is able to achieve a better accuracy but PUFEM is slightly better conditioned when the wave is not well resolved. However, with a sufficient wave resolution, BBFEMs is better conditioned than PUFEM. Results from L-shaped domain problem, with non quasi-uniform mesh grids, show that the conditioning of BBFEMs remains reasonable while PUFEM with large numbers of enriching plane waves on mesh grids locally well resolved leads to ill-conditioning.

bold Keywords
Wave problems; finite elements; Bernstein-Bézier; plane waves; Helmholtz equation; high frequency

1 Introduction

The Helmholtz equation describes many wave problems in the frequency domain including wave propagation, guiding, radiation and scattering. Owing to its ability in handling complex geometries, material heterogeneity and anisotropy, the Finite Element Method (FEM) plays a key role in a wide range of applications in acoustics, optics and electromagnetics, such as radar cross section prediction, acoustic noise control and seismic wave propagation. However, designing an efficient and reliable approximation method for wave problems at high frequency, where the pollution error dominates the overall error of the FE solution, remains a crucial issue. With low order conventional FE, the method requires many nodal points per wavelength to achieve an acceptable accuracy, and hence yields prohibitively large computational costs. The works [1–3] have clearly shown the challenging issues that are confronted when the finite element is used for solving the Helmholtz equation. Related studies dealing with the dispersion behaviour of *hp*-FEM and high order Discontinuous Galerkin (DG) methods can be found in [4, 5].
With the aim to reduce the pollution effect, high order methods have been developed to cope with

frequency limitation and high resolution requirement of low order methods. These include polynomial based methods relying on the use of high order shape functions such as Lobatto, Bernstein and Hermite polynomials or spectral elements. Assessment of various polynomial shape functions, including Lagrange Gauss-Lobatto, integrated Legendre and Bernstein polynomials, for interior acoustic problems in [6] have shown the advantage of high order polynomials in reducing the pollution error and the good performance of Bernstein polynomials when combined with Krylov subspace solvers. It was concluded, however, that the stability of Krylov subspace methods deteriorates as the polynomial order increases. Comparison studies with an emphasis on conditioning indicate that high order elements based on Bernstein polynomials lead to low conditioning for the Laplace operator [7]. The studies also indicate that condensed hierarchic finite elements lead to stiffness matrices with better condition number than that of Gauss-Lobatto based spectral elements [8]. The above mentioned investigations show that the choice of the polynomial FE basis is critical to the stability and efficiency of the FE procedure. From a computational viewpoint, hierarchical basis are often preferred when using the p-adaptivity. In fact, it is not required to reconstruct the entire basis when the polynomial order is increased. High-order Lobatto polynomials were successfully developed for two dimensional Helmholtz problems and three-dimensional acoustic applications in [9, 10] and extended to the convected Helmholtz equation in [11]. A comparison study of the performance of high order continuous and DG methods for two dimensional scattering problems was performed in [12]. Related work dealing with complexity analysis in solving the resulting linear systems is carried out in [13].

Another alternative to reduce the pollution effect has been the use of wave-based methods. The common idea in these approaches is to include *a priori* knowledge about the wave behaviour in the numerical scheme. For Helmholtz problems, this is usually achieved by incorporating plane waves or Bessel functions locally in the approximated solution. These methods include the partition of unity method [15–18], the generalised finite element method [21, 22], the variational theory of complex rays [29] and other methods based on a DG framework such as the least-squares method [14], the ultra weak variational formulation [19, 20] and the discontinuous enrichment method [23, 24]. For comparative studies of the performance of such methods see [30, 31]. Other enrichment methods relying on the DG framework are the oscillated FE polynomials [25] and the stable DG method [26]. Note that these methods differ from each other by the way inter-element continuity is enforced. Wave based methods were also developed within the framework of the boundary element method such as the partition of unity boundary element method [27] or the isogeometric wave-enriched boundary element method [28].

The use of wave based methods is generally justified by the fact that the enriching wave functions are solutions of the underlying equations and hence lead to better accuracy results compared to polynomial based methods. A comparative study in [9] dealing with two-dimensional Helmholtz problems shows that high order polynomial methods lead to comparable accuracy provided by wave-based methods, or even better accuracy in some cases. Results obtained by the Spectral Element Method (SEM) based on high order Lagrangian shape functions with Chebyshev-Gauss-Lobatto nodal distribution were compared against PUFEM results in [32]. The case involving evanescent waves indicates that SEM is able to achieve good accuracy but with a higher discretization level compared to PUFEM.

Bernstein polynomials are widely used in the field of computer aided geometric design and computer graphics. However, their use in the finite element community is generally investigated to a lesser extent. Besides the works [6, 7] mentioned previously, simplicial Bernstein-Bézier FEs have recently been studied in [42, 43] with emphasis on fast procedures for evaluating mass and stiffness matrices. Closely related studies in [44, 45] show that high order Bernstein-Bézier FEs over simplicial domains, hexahedra and pyramids, can yield optimal complexity for the standard FE spaces.

The present work focuses on the implementation and performance of high order Bernstein-Bézier FEs for solving Helmholtz problems on unstructured mesh grids. This high order scheme is constructed from the six-noded triangular element, where the mid-side nodes are used to represent the edge degrees of freedom of Bernstein-Bézier elements. To carry out a fair comparison against PUFEM, the resulting global matrices from both methods are assembled using coordinate storage format and the same sparse direct solver is used for the solution of the corresponding linear systems. These of course require additional work on the PUFEM code that previously uses a steering vector to locate global matrix entries and a profile matrix solver [46]. Three benchmark problems are dealt with to provide a detailed comparison of these two higher-order methods in terms of accuracy, conditioning and memory requirement.
The outline of the paper is as follows: After introducing the model problem in Section 2, detailed descriptions of PUFEM and BBFEM are presented in Section 3. An overview of the solution method is given in Section 4. In section 5, the benchmark problems and measures of performance are described, followed by a comparison study of the performance of both higher-order methods. Finally some concluding remarks are drawn in Section 6.

2 The model problem

For the sake of simplicity, we restrict ourselves to the following model problem governed by the Helmholtz equation

$$-k^2 u - \Delta u = 0 \quad \text{in} \quad \Omega \tag{1}$$

$$\nabla u \cdot \mathbf{n} + \mathrm{i}ku = g \quad \text{in} \quad \Gamma, \tag{2}$$

where Ω is a bounded domain in $\mathbb{R}^2$, with a Lipschitz continuous and piecewise smooth boundary Γ, $\mathbf{n}$ is the outer normal unit vector to Γ, g is a boundary data in $L^2(\Gamma)$, $k > 0$ is the wavenumber and i is the imaginary unit.
Multiplying Equation (1) by a test function v, integrating by parts over Ω and taking into account (2), yields the weak form of (1)-(2):

$$-k^2 \int_\Omega u\bar{v}\, \mathrm{d}\Omega + \int_\Omega \nabla u \cdot \nabla \bar{v}\, \mathrm{d}\Omega + \mathrm{i}k \int_\Gamma u\bar{v}\, \mathrm{d}\Gamma = \int_\Gamma g\bar{v}\, \mathrm{d}\Gamma, \quad \forall v \in H^1(\Omega), \tag{3}$$

where $\bar{v}$ is the complex conjugate of the test function v. Sound-soft (resp. sound-hard) boundary condition, where u (resp. $\nabla u \cdot \mathbf{n}$) is prescribed at a part of the boundary Γ may be used, and an absorbing boundary or the Sommerfeld radiation condition may also be included in the case of exterior domains. It is worth noting that PUFEM has been successfully implemented with exact and approximate non-reflecting boundary conditions in [33]. To avoid additional sources of numerical error in modeling an unbounded domain or curved boundary, when a high order discretisation method is performed, a Robin boundary condition (2) is introduced to impose the exact solution. Existence and uniqueness results for the variational problem (3) can be established by using Fredholms alternative theorem [34] and continuation arguments [35].

3 High order discretisations

As usually done in FEM, the domain Ω is partitioned into a set of non-overlapping finite elements T_e. The discretisation parameter of the mesh grid is denoted by h. Since practical wave problems may

involve domains with curved boundaries, the finite elements considered in this study are six-noded triangles. Let $\hat{T}$ be the reference element defined by

$$\hat{T} = \{\boldsymbol{\xi} = (\xi_1, \xi_2) : \quad 0 \leq \xi_1 \leq 1, \quad 0 \leq \xi_2 \leq 1 - \xi_1\}. \tag{4}$$

The geometry is described by the mapping $\boldsymbol{x} = \Phi_e(\boldsymbol{\xi})$ between the global coordinates $\boldsymbol{x} = (x_1, x_2)$ and the local coordinates $\boldsymbol{\xi} = (\xi_1, \xi_2)$:

$$\Phi_e(\boldsymbol{\xi}) \quad = \quad \sum_i \lambda_i(\boldsymbol{\xi})(2\lambda_i(\boldsymbol{\xi}) - 1)\boldsymbol{q}_i + 4\sum_{i<j} \lambda_i(\boldsymbol{\xi})\lambda_j(\boldsymbol{\xi})\boldsymbol{q}_{ij}, \tag{5}$$

where $\boldsymbol{q}_i$ and $\boldsymbol{q}_{ij}$ are the nodes of T_e and λ_i, $i = 1, \cdots, 3$ are the barycentric coordinates relative to the reference element $\hat{T}$ given by,

$$\lambda_1(\boldsymbol{\xi}) = \xi_1, \quad \lambda_2(\boldsymbol{\xi}) = \xi_2 \quad \text{and} \quad \lambda_3(\boldsymbol{\xi}) = 1 - \xi_1 - \xi_2. \tag{6}$$

The important point to notice here is that the mapping Φ_e becomes affine if the nodes $\boldsymbol{q}_{ij}$ are exactly the mid-points $\frac{\boldsymbol{q}_i + \boldsymbol{q}_j}{2}$.
The following subsections describe the high order dicretisation schemes used in this paper.

3.1 BBFEM approximation

In order to introduce Bernstein polynomials, multi-index notations are introduced. A d-dimensional multi-index $\boldsymbol{\alpha}$ in $\mathbb{Z}_+^d$ is a d-tuple $\boldsymbol{\alpha} = (\alpha_1, \alpha_2, \cdots, \alpha_d)$ of non-negative integers. The order of a multi-index $\boldsymbol{\alpha}$, written $|\boldsymbol{\alpha}|$ is given by $|\boldsymbol{\alpha}| = \sum_{i=1,d} \alpha_i$. For a given pair $\boldsymbol{\alpha}$, $\boldsymbol{\beta}$ in $\mathbb{Z}_+^d$, their sum and difference are defined component-wise by

$$\boldsymbol{\alpha} \pm \boldsymbol{\beta} = (\alpha_1 \pm \beta_1, \alpha_2 \pm \beta_2, \cdots, \alpha_d \pm \beta_d).$$

The factorial of a multi-index is defined by $\boldsymbol{\alpha}! = \prod_{i=1,d} \alpha_i!$. The binomial and multinomial coefficients are defined by

$$\left(\begin{array}{c} \boldsymbol{\alpha} \\ \boldsymbol{\beta} \end{array} \right) = \frac{\boldsymbol{\alpha}!}{(\boldsymbol{\beta} - \boldsymbol{\alpha})!}, \quad \left(\begin{array}{c} |\boldsymbol{\alpha}| \\ \boldsymbol{\alpha} \end{array} \right) = \frac{|\boldsymbol{\alpha}|!}{\boldsymbol{\alpha}},$$

respectively. For $\boldsymbol{\xi} \in \mathbb{R}^d$, the power is defined by $\boldsymbol{\xi}^{\boldsymbol{\alpha}} = \prod_{i=1,d} \xi_i^{\alpha_i}$. Let us denote by $\mathbb{P}^p(\hat{T})$ the space of polynomials of total degree at most p. The Bernstein polynomials of degree $p \in \mathbb{Z}_+$ associated with the reference element $\hat{T}$, are defined by

$$B_{\boldsymbol{\alpha}}^p(\boldsymbol{\xi}) = \left(\begin{array}{c} p \\ \boldsymbol{\alpha} \end{array} \right) \boldsymbol{\lambda}^{\boldsymbol{\alpha}}(\boldsymbol{\xi}), \quad \text{with} \quad \boldsymbol{\alpha} \in \mathcal{I}_2^p, \tag{7}$$

where $\boldsymbol{\lambda}(\boldsymbol{\xi}) = (\lambda_1(\boldsymbol{\xi}), \lambda_2(\boldsymbol{\xi}), \lambda_3(\boldsymbol{\xi}))$ and $\mathcal{I}_2^p$ is the index set

$$\mathcal{I}_2^p = \{\boldsymbol{\alpha} \in \mathbb{Z}_+^3 : |\boldsymbol{\alpha}| = p\}. \tag{8}$$

Bernstein polynomials have many interesting properties: They form a basis of the space $\mathbb{P}^p(\hat{T})$, are non-negative and form a partition of unity on $\hat{T}$. The BBFEM solution u_h is sought element-wise under the B-form

$$u_h(\boldsymbol{x}) = \sum_{\boldsymbol{\alpha} \in \mathcal{I}_2^p} u_{\boldsymbol{\alpha}} B_{\boldsymbol{\alpha}}^p(\boldsymbol{\xi}). \tag{9}$$

The properties of bivariate polynomials defined on a triangle and written in the B-form are addressed in [36]. These cover practical aspects related to the efficient evaluation of polynomials, their derivatives, integrals and inner products.
At the element level, a numbering scheme of the local DoF should be used. For example, in the case of a polynomial order $p = 4$, the numbering adopted here is illustrated in Figure 1.

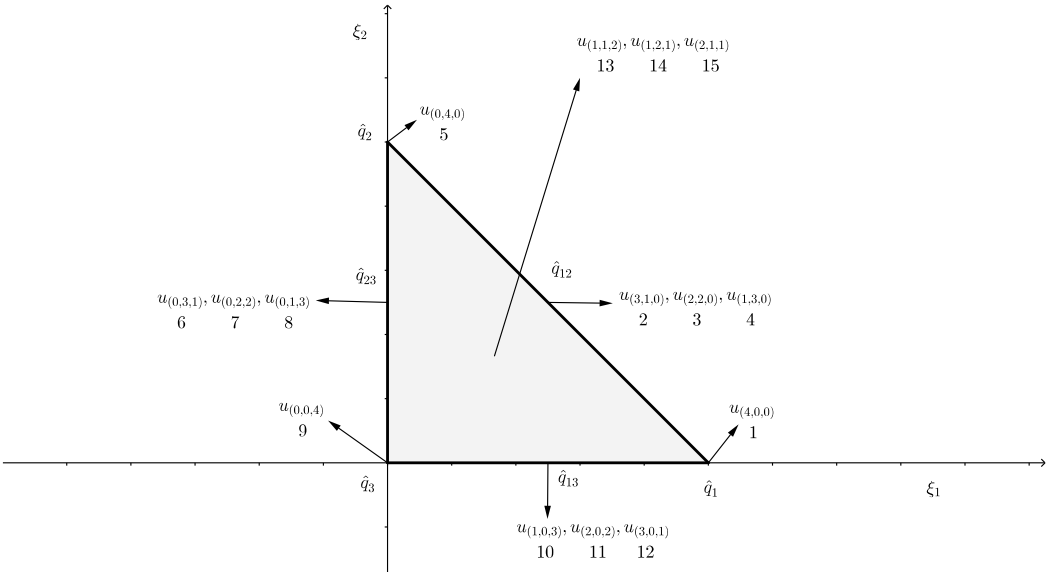

Figure 1: Numbering scheme of the local degrees of freedom.

Vertex nodes have only one degree of freedom , namely, 1, 5 and 9, respectively. The mid-point nodes (or the edges) possess $p - 1 = 3$ DoF. For instance, DoF attached to the edge $(\hat{q}_1\hat{q}_3)$ are 10, 11 and 12. The element interior DoF 13, 14 and 15 have cardinality $\frac{(p-2)(p-1)}{2} = 3$ and interact only with the element itself and its nodes.
As for the classical H^1-conforming p-FEM with hierarchical shape functions, the local Bernstein shape functions given by (7) can be classified into three categories, which are the vertex, edge, and bubble functions. The above structure of the local DoF is well adapted to a six-nodes triangular mesh grid. For a polynomial order $p \geq 3$, the number of DoF per element is given by

$$n^e_{\text{dof}} = 3 + 3(p-1) + \frac{(p-2)(p-1)}{2}. \tag{10}$$

Bernstein polynomials provide a completely natural basis for non-uniform order polynomial approximation [37], where different polynomial orders may be attached to vertices, edges and the element interior. The C^0 conformity of BBFEM is ensured by matching edge modes of a similar shape, based on a global orientation of the FE edges (see [38, 39] for further details).
The global numbering convention used here consists in numbering all nodes first, where the mid-points are used for the global edges, followed by the interior modes. This scheme is more suited for the static condensation, which consists in removing interior modes from the resulting discrete algebraic system during the assembling process. Once the solution related to the vertex and edge modes is known, the solution for the interior modes can be recovered by solving small linear algebraic systems at an elemental level. This technique is very efficient in reducing the total DoF and bandwidth of hp FE matrices.

3.2 PUFEM approximation

Here, a brief description of PUFEM is given. The six-noded local shape functions of the reference element $\hat{T}$ defined by (4), which form a partition of unity, are enriched by using plane waves. The PUFEM solution is defined on an element T_e by

$$u_h = \sum_i \sum_{l=1}^{m_{\underline{i}}} u_i^l \exp\left(\mathrm{i}k\boldsymbol{x}\cdot\boldsymbol{d}_{\underline{i}}^l\right)\varphi_i + \sum_{i<j}\sum_{l=1}^{m_{\underline{i},\underline{j}}} u_{i,j}^l \exp\left(\mathrm{i}k\boldsymbol{x}\cdot\boldsymbol{d}_{\underline{i},\underline{j}}^l\right)\varphi_{i,j}, \tag{11}$$

where $\varphi_i = \lambda_i(\boldsymbol{\xi})(2\lambda_i(\boldsymbol{\xi})-1)$, $\varphi_{i,j} = 4\lambda_i(\boldsymbol{\xi})\lambda_j(\boldsymbol{\xi})$, $\underline{i} = \sigma_e(i)$ and σ_e is the element mapping from local to global node numbers. For simplicity, the unit plane wave directions $\boldsymbol{d}_{\underline{i}}^l$ and $\boldsymbol{d}_{\underline{i},\underline{j}}^l$ attached to vertex and mid-point nodes, respectively, are chosen to be uniformly distributed on the unit circle. The unknowns are here the wave amplitudes u_i^l and $u_{i,j}^l$. When a uniform enrichment by plane waves is used, i.e., $m_{\underline{i}} = m_{\underline{i},\underline{j}}$ for all nodes of the mesh grid, the parameter m is used for referring to the common number of plane waves. At the element level, DoF are numbered in a natural way as illustrated in Figure 2 and the C^0 conformity of PUFEM is ensured.

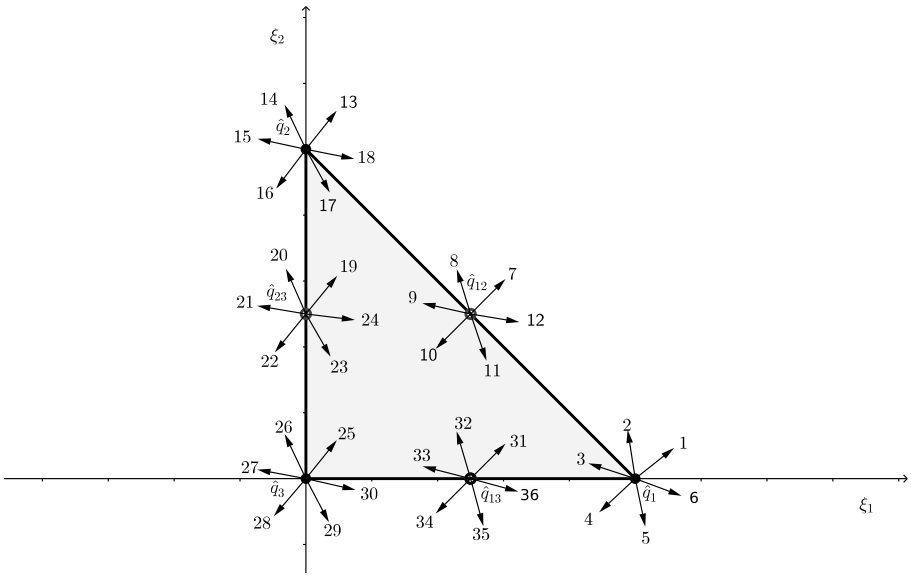

Figure 2: Numbering scheme of the local degrees of freedom (case $m = 6$ shown).

The relative hp-FE error for Helmholtz problems in the H^1-seminorm, on a uniform hp-mesh, is bounded by [2]

$$\frac{|u-u_h|_1}{|u|_1} \leq C_1\left(\frac{kh}{2p}\right)^p + C_2 k\left(\frac{kh}{2p}\right)^{2p}, \tag{12}$$

where the constants C_1 and C_2 are independent of kh. The first term on the right hand side in (12) scales as the best approximation error. The second term is linked to the numerical pollution. It is clearly seen from (12) that the overall error is dominated by this last term at high wave numbers. Moreover, the pollution effect for $p \geq 2$ is significantly reduced if $\frac{kh}{2p}$ is small enough.

Suppose Ω is a simply connected bounded Lipschitz domain, star-shaped with respect to a ball and that the exterior angle of Ω is bounded below by $\lambda\pi$, where $0 < \lambda < 1$. Then, for any solution $u \in H^s(\Omega)$, with $s > 1$, of the homogeneous Helmholtz equation, the following approximation

property holds [40]

$$\inf_{u_m \in W(m)} \|u - u_m\|_1 \leq C \left(\frac{\ln^2 m}{m} \right)^{\lambda(s-1)} \|u\|_s, \tag{13}$$

where the constant C depends only on Ω, s and k. Here, $H^s(\Omega)$ is the usual Sobolev space of real order s, endowed with its norm $\|\cdot\|_s$ and $W(m)$ is the space spanned by m plane waves, chosen uniformly distributed on the unit circle. Estimate (13) does not give an idea about the stability of PUFEM. However, as it is well known from numerical experiments, this method performs very well at a high wavenumber, for multi-wavelength sized elements.

4 Solution method

The approximation of the weak form (3) by either BBFEM or PUFEM yields the following algebraic linear system

$$\boldsymbol{A}\boldsymbol{u} = \boldsymbol{b}, \tag{14}$$

with $\boldsymbol{A}$ is a $n_{\text{dof}} \times n_{\text{dof}}$ sparse, complex symmetric matrix and $\boldsymbol{b}$ is the right-hand side column vector of $\mathbb{C}^{n_{\text{dof}}}$, where n_{dof} is the total number of DoF, and $\boldsymbol{u}$ is the unknown column vector of DoF. Let us point out that the unconjugated formulation was used in PUFEM to guarantee the symmetry of $\boldsymbol{A}$.
The global matrix $\boldsymbol{A}$ and the right-hand side $\boldsymbol{b}$ entries are evaluated by assembling , in (symmetric) coordinate format, the element contribution $\boldsymbol{A}_e$ and $\boldsymbol{b}_e$. The element matrix has the following form

$$\boldsymbol{A}_e = -k^2 \boldsymbol{M}_e + \boldsymbol{K}_e + \mathrm{i}k \boldsymbol{S}_e. \tag{15}$$

Denoting by $\boldsymbol{\varphi}_e$ the column vector of the local shape functions, the element mass and stiffness matrices in (15) can be written as

$$\boldsymbol{M}_e = \int_{\hat{T}} \boldsymbol{\varphi}_e \boldsymbol{\varphi}_e^\top \det(\boldsymbol{J}_e)\, \mathrm{d}\boldsymbol{\xi} \tag{16}$$

$$\boldsymbol{K}_e = \int_{\hat{T}} \left[\boldsymbol{J}_e^{-1} \nabla \boldsymbol{\varphi}_e\right] \left[\boldsymbol{J}_e^{-1} \nabla \boldsymbol{\varphi}_e\right]^\top \det(\boldsymbol{J}_e) \mathrm{d}\boldsymbol{\xi}. \tag{17}$$

The element matrix $\boldsymbol{S}_e$ and right hand side $\boldsymbol{b}_e$ are evaluated as

$$\boldsymbol{S}_e = \int_0^1 \boldsymbol{\varphi}_e \boldsymbol{\varphi}_e^\top J_e^\Gamma \, \mathrm{d}t \tag{18}$$

$$\boldsymbol{b}_e = \int_0^1 g \boldsymbol{\varphi}_e J_e^\Gamma \, \mathrm{d}t. \tag{19}$$

Here $\boldsymbol{J}_e = \left(\frac{\mathrm{D}\Phi_e}{\mathrm{D}\boldsymbol{\xi}}\right)^\top$ denotes the Jacobian matrix, t is the parameter describing the edge parametric curve $\hat{\Gamma}_e = \Phi_e^{-1}(\Gamma_e)$, where Γ_e is a physical edge lying on the Robin boundary, and $J_e^\Gamma = \sqrt{x_1'^2(t) + x_2'^2(t)}$, with the prime denoting the derivative with respect to t.
The element integrals in expressions (16)-(19) are evaluated using high order Gauss-Legendre integration scheme. A large number of quadrature points will be needed, because of the presence of high order polynomials and highly oscillating wave functions in the integrands of BBFEM and PUFEM, respectively. It is worthwhile noting that for elements with straight edges the mapping Φ_e

becomes affine, as previously mentioned, and analytical integration rules for BBFEM integrands as discussed in [43, 44] may be used. For PUFEM integrands, the approach developed in [41] can be extended to the six-noded element. In the presence of curved elements and/or varying coefficients, the order of quadrature has to be increased to further capture the variation of the Jacobian and involved coefficients. Fast quadrature procedures, based on the use of collapsed coordinates, which take advantage of sum factorisation, are investigated in [43, 44], but they are not used in this work.

5 Numerical examples

In this section, benchmark problems and measures of performance of BBFEM and PUFEM are described. Then a comparison study on the performance of both high order methods is carried out in terms of accuracy, conditioning and memory requirements.

5.1 Description of the benchmark tests

Three benchmark problems are considered to assess the performance of BBFEM and PUFEM in terms of convergence, conditioning and memory requirements. These numerical tests involve analytical solutions enforced by using the Robin boundary condition (2). Examples of these solutions are depicted for illustration purpose in Figure 3.

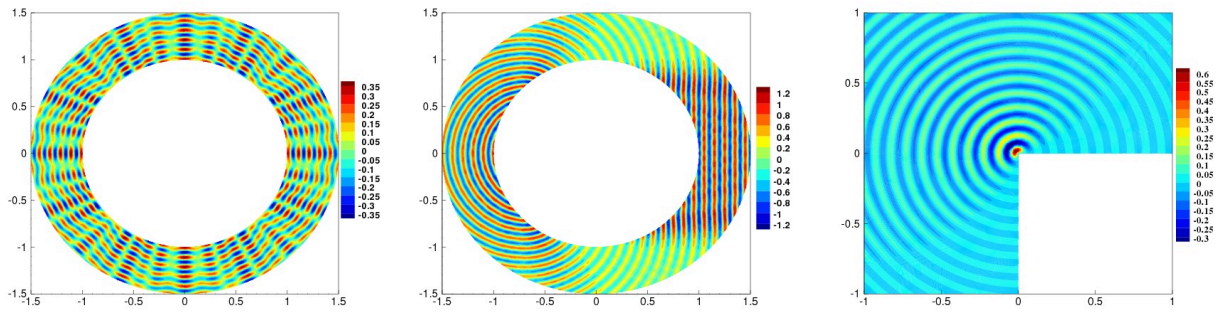

Figure 3: Examples of analytical solutions of the three benchmark problems, with $ka = 20\pi$: Hankel sources (left), wave scattering (middle) and L-shaped domain (right).

The first benchmark problem deals with the interference of four radial sound sources placed at different locations. The computational domain Ω has an annular shape with inner and outer radii R and $R + a$, respectively. The sound sources are located at $\boldsymbol{s}_1 = (0, -0.5)$, $\boldsymbol{s}_2 = (0.5, 0)$, $\boldsymbol{s}_3 = (0, 0.5)$ and $\boldsymbol{s}_4 = (-0.5, 0)$, and the analytical solution is given as the following sum of Hankel functions of first kind and order zero

$$u_a \quad = \quad \sum_{i=1,4} \mathrm{H}_0(k|\boldsymbol{x} - \boldsymbol{s}_i|_2), \tag{20}$$

where $|\cdot|_2$ is the usual l_2 norm. A sequence of ten mesh grids were used for this benchmark. The coarse mesh grid M_1 of Figure 4 which has a mesh size $h = 0.75a/2$ is gradually refined by using a global refinement factor $f_n = 0.75a/n$, with $n = 4, 6, \cdots, 18, 20$.

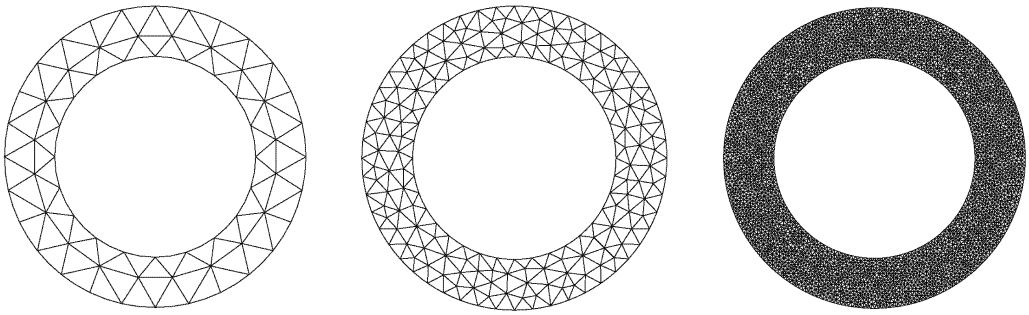

Figure 4: Typical unstructured mesh grids: M_1, $h = 0.75a/2$ (left), $M_{1/2}$, $h = 0.75a/4$ (middle) and M_f, $h = 0.75a/20$ (right).

The second benchmark problem concerns the scattering of a horizontal plane wave by a rigid circular cylinder of unit radius a, centered at the origin. The computational domain Ω is the same as the one previously considered in the first benchmark, and the analytical solution is given by

$$u_a = -\sum_{m=0}^{\infty} \epsilon_m \mathrm{i}^m \frac{\mathrm{J}'_m(ka)}{\mathrm{H}'_m(ka)} \mathrm{H}_m(kr)\cos(m\theta), \tag{21}$$

where (r, θ) denotes the polar coordinates system, $\epsilon_0 = 1$, $\epsilon_m = 2$ for $m \geq 1$, J_m and H_m are respectively the Bessel and Hankel functions of the first kind and order m. The infinite expansion involved in (21) is truncated and a finite number of terms, denoted N_t, is chosen such that $N_t \simeq ka$. It is well known that the performance of high order methods deteriorates substantially with the presence of non-smooth solutions. Both high order FE [51] and wave based [9, 55] methods fail to achieve a fast convergence. The specific case examined here is a non-smooth wave problem due to a re-entrant corner. The analytical solution is given by

$$u_a = \mathrm{J}_\alpha(kr)\sin(\alpha\theta), \quad 0 \leq \theta \leq \frac{\pi}{\alpha},$$

where $\alpha = 2/3$ and J_α is the Bessel function of the first kind, with a non integer order α. Since $\alpha < 1$, the first derivatives of u_a have a singularity at the origin. In contrast with the previous benchmarks, where analytical regularity holds, the Helmholtz solution of the L-shape domain problem has only $H^{\alpha+1-\epsilon}(\Omega)$ regularity (for any $\epsilon > 0$) [47]. For such type of problems, the convergence rate of high order methods deteriorates. To alleviate this issue, local quasi-uniform meshing with refinement around the re-entrant corner is used. References on alternative approaches, such as geometrical mesh refinement, conformal mappings and enrichment methods, with basis functions including the form of singularity, can be found in [38].
Four mesh grids are used for this benchmark problem (see Figure 5). The mesh grid M_{I}^L is gradually refined by a factor of $1/10$ around the re-entrant corner $(0, 0)$.

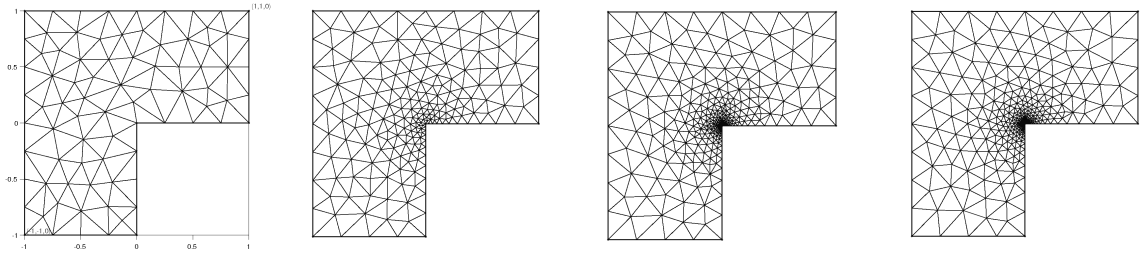

Figure 5: Typical unstructured non quasi-uniform mesh grids of the L-shaped domain: M_i^L (left), $i = 1, \cdots, 4$.

5.2 Measures of Performance

The benchmarks described above depend on a number of parameters; namely, the wavenumber k, the mesh size h, the polynomial order p and the number of plane waves m. When keeping the mesh grid fixed, q-refinement refers to the increase or the decrease of either p or m. The wave resolution is measured by

$$\tau_\lambda = \lambda \sqrt{\frac{n_{\text{dof}}}{|\Omega|}}, \tag{22}$$

where $|\Omega|$ is the surface area of Ω. The indicator τ_λ represents the number of DoF per wavelength λ. Let us point out that when BBFEMs (with static condensation) is used, the internal bubble degrees of freedom are not included in n_{dof}. The accuracy of the numerical solution is assessed by the following relative L^2 error

$$\varepsilon_2 = \frac{\|u_h - u_a\|_0}{\|u_a\|_0} \times 100\%, \tag{23}$$

where $\|\cdot\|_0$ is the usual norm of $L^2(\Omega)$. Both BBFEM and PUFEM yield a sparse linear system, with a symmetric complex valued matrix. The resulting linear system is solved by using the multi-frontal sparse direct solver MUMPS [48], interfaced with METIS package [49] to reduce the bandwidth and the extra fill-in of the global matrix. To assess the cost of the solution processing, the following outputs provided by MUMPS are reported:

- The number nnz of non-zero entries in the global matrix.
- The number n_f of entries in factors.
- The space in MBytes needed during the factorisation step.

Although high order methods lead to a high level of accuracy, computing the solution of their associated linear systems can be challenging, because of the specific sparsity pattern and large bandwidth of the resulting global matrix.

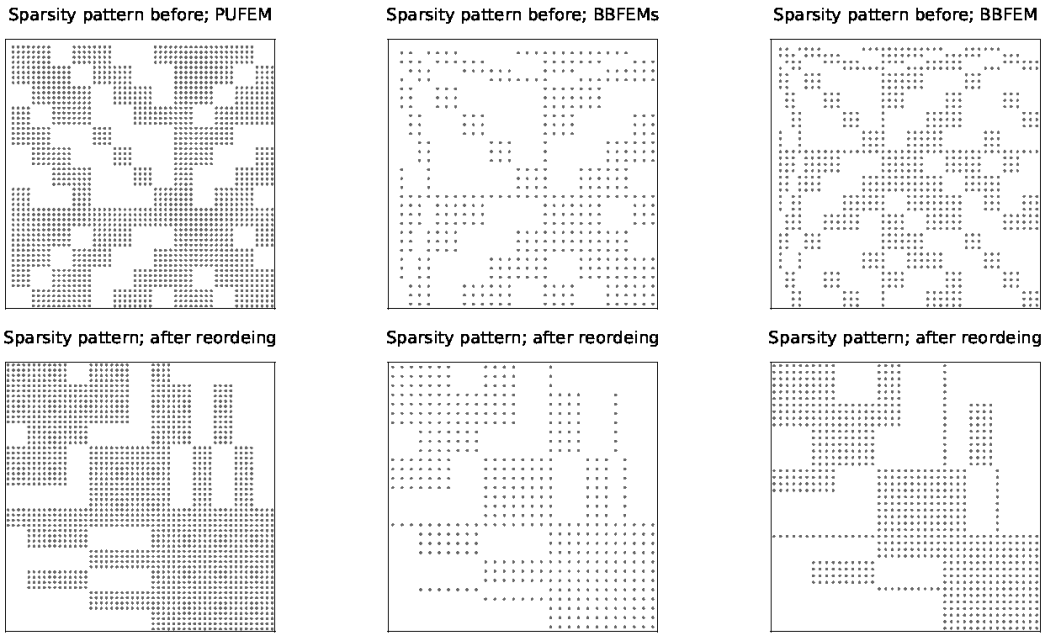

Figure 6: Examples of sparsity pattern of the global matrices before and after METIS based reordering: PUFEM (left), BBFEMs (middle), BBFEM (right).

Sparsity patterns of Figure 6 were obtained for a mesh grid of a square domain consisting of 4 elements and 13 nodal points, with $m = p = 4$. It is obvious that PUFEM has a denser sparsity pattern compared to BBFEM and BBFEMs. Moreover, with the help of static condensation, the total number of DoF needed in BBFEM is significantly reduced. The advantage of reordering in reducing the bandwidth is clearly seen.
When a sparse direct solver is used, the numerical pivoting may lead to significant extra fill-in. To investigate this issue, the percentage of fill-in in the global matrix defined by

$$p_f = \frac{n_f}{n_{\text{dof}}^2 - nnz} \times 100\% \tag{24}$$

is introduced. Another useful indicator is the condition number of the resulting linear system, it is also provided by MUMPS solver and is given by

$$\kappa_{A,b} = \frac{\| \, |\boldsymbol{A}| \, |\boldsymbol{A}^{-1}| \, |\hat{\boldsymbol{x}}| + |\boldsymbol{A}^{-1}| \, |\boldsymbol{b}| \, \|_\infty}{|\hat{\boldsymbol{x}}|_\infty}, \tag{25}$$

where $\hat{\boldsymbol{x}}$ is the calculated solution, $|\cdot|_\infty$ is the usual l_∞ norm, $|\boldsymbol{A}| = (|\boldsymbol{A}_{ij}|)$ and $|\boldsymbol{b}| = (|\boldsymbol{b}_i|)$. Further details on the above condition estimate can be found in [50].

5.3 Interference of Hankel sources

For this problem, dealing with the interference of Hankel sources, two types of analysis are carried out. In the first analysis, the polynomial order p for BBFEM and the number m of approximating plane waves are increased. In the second analysis, the influence of the mesh size h is considered.

5.3.1 Convergence and conditioning analysis: q-refinement

First, a comparison study of BBFEM and BBFEMs is presented. The numerical experiments are performed on the coarse mesh grid M_1 (see Figure 4), at fixed wavenumbers $ka = 10\pi$ and $ka = 15\pi$,

by increasing the polynomial order p. The relative L_2 error ε_2 and the condition number $\kappa_{A,b}$ are plotted against p in Figure 7, for the wavenumber $ka = 10\pi$.

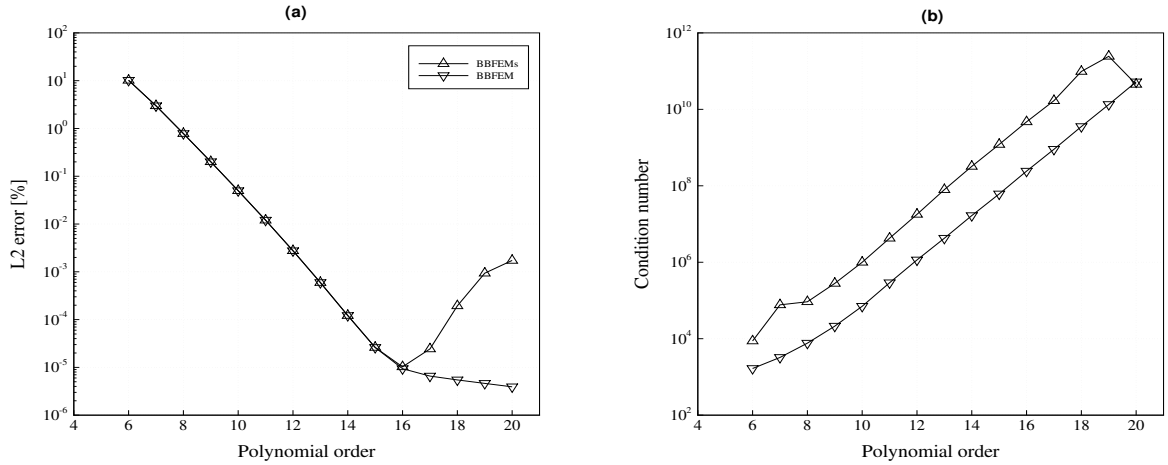

Figure 7: The L^2 error (left) and condition number (right) versus p; $h = 0.75a/2$ and $ka = 10\pi$.

It is observed on Figure 7(a) that BBFEM and BFFEMs lead to similar convergence results. Moreover, the relative L_2 error of both schemes decays exponentially, provided the order p is below a prescribed upper bound. As expected for high order methods, the condition number grows exponentially with the polynomial order p (see Figure 7(b)). At a first glance, it is expected to obtain a low condition number, when static condensation is performed, but the results of Figure 7(b) show that the condition number of BBFEMs is higher than that of BBFEM by one order of magnitude. With further increase of the polynomial order, $p > 16$, the effect of ill-conditioning is clearly seen with a slow decay of the relative L_2 error of BBFEM and its deterioration when static condensation is used. These results indicate that this procedure which involves the inversion of the block matrix

$$\boldsymbol{B}_e \;=\; -k^2 \int_{\hat{T}} \boldsymbol{\varphi}_e^b \boldsymbol{\varphi}_e^{b\top} \det(\boldsymbol{J}_e)\, \mathrm{d}\boldsymbol{\xi} + \int_{\hat{T}} \left[\boldsymbol{J}_e^{-1} \nabla \boldsymbol{\varphi}_e^b\right] \left[\boldsymbol{J}_e^{-1} \nabla \boldsymbol{\varphi}_e^b\right]^\top \det(\boldsymbol{J}_e)\, \mathrm{d}\boldsymbol{\xi}, \tag{26}$$

may suffer from ill-conditioning for high polynomial orders. Note that $\boldsymbol{B}_e$ is nearly singular if k^2 is an eigenvalue of the Dirichlet Laplacian operator. Here $\boldsymbol{\varphi}_e^b$ is the column vector of bubble local shape functions. Following an idea developed in [57], a rule to avoid a breakdown of condensation may be obtained. For simplicity, suppose T_e is a triangle with straight edges. Using Pólya's inequality [58]

$$\mu_1 |T_e| \geq \frac{4\pi^2}{\sqrt{3}}, \tag{27}$$

which gives a lower bound on the first Dirichlet eigenvalue, and the fact that $\mu_1^h \geq \mu_1$ and $|T_e| \leq h^2$, a sufficient condition to avoid a breakdown of condensation is

$$kh \ll 2\pi \sqrt{\frac{1}{\sqrt{3}}} \simeq 1.52\pi. \tag{28}$$

This ill-conditioning issue is very pronounced for high polynomial order p with a poor grid resolution on a coarse mesh, where the discrete resonant frequencies of $\boldsymbol{B}_e$ have cardinality equal to

$(p-2)(p-1)/2$. In practice, as the polynomial order increases, the computational cost of eliminating and recovering bubble degrees of freedom grows substantially and may dominate the overall computational cost of the solution process. Moreover, the computational cost of the full BBFEM use, without condensation, is noticeable because the order of the bubble block matrices scales as p^2 and yields a global matrix with a large bandwidth. Therefore, it is believed that BBFEMs may guarantee a trade off between efficiency and accuracy, provided a moderate polynomial order is used. In 3D applications, where the order of the bubble block matrices scales super-linearly as p^3, static condensation can be efficiently performed in parallel to mitigate the computational burden related to the elimination and recovery of condensed degrees.

Similar numerical experiments are conducted by further increasing the wavenumber ka to 15π and using mesh grid $M_{1/2}$, whose elements may contain up to $h/\lambda \simeq 2.81$ wavelengths. Results of Figure 8(a) exhibit the same trend shown previously. However, the exponential rate of decay of the L_2 error is lower, compared with the case of Figure 7(a). This is not surprising because, for a fixed grid resolution, the polynomial order has to be further increased as the wavenumber increases to achieve a given accuracy. Although the condition number of BBFEMs is comparable to that of BBFEM, with some low amplitude peaks (see Figure 8(b)), the accuracy of BBFEMs deteriorates for large polynomial orders. An in-depth investigation of the bubble matrix $\boldsymbol{B}_e$ spectrum may help to understand the behaviour of the conditioning of BBFEMs with respect to the wavenumber, polynomial order and element mesh size.

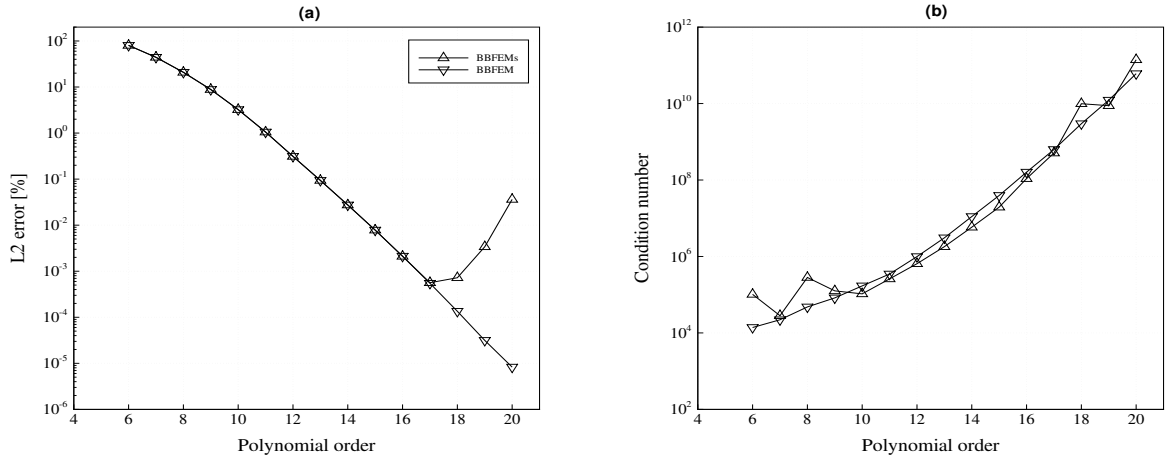

Figure 8: The L^2 error (left) and condition number (right) versus p; $h = 0.75a/2$ and $ka = 15\pi$.

Next, the performance of BBFEMs is compared against PUFEM in terms of convergence rate, conditioning and memory requirement. The same parameters for the mesh grid and wavenumber are used. At a fixed mesh size $h = 0.75a/2$ and wavenumber ka, the polynomial order p and number m of plane waves are increased. In Figure 9, the condition number $\kappa_{A,b}$ and number nnz of non zero entries in the global matrix are plotted against the L^2 error ϵ_2, for the wavenumber $ka = 10\pi$. In the preasymptotic region, i.e., $\epsilon_2 \geq 0.1\%$, both BBFEMs and PUFEM lead to a comparable level of the conditioning while, on the contrary, the conditioning of PUFEM is up to four orders of magnitude larger than that of BBFEMs in the asymptotic region (see Figure 9(a)). A notable saving is also achieved, in term of the number of non zero entries in the global matrix of BBFEMs (see Figure 9(b)).

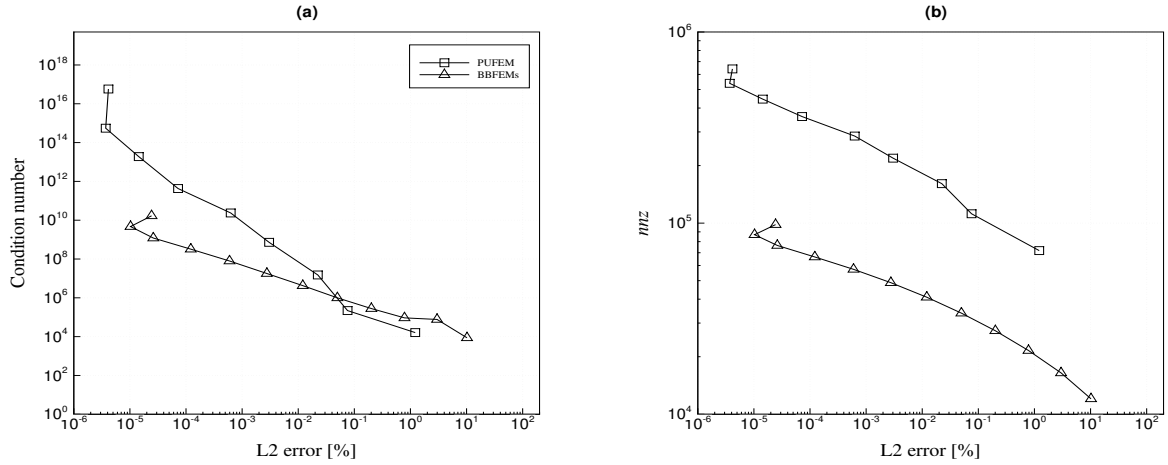

Figure 9: The condition number (left) and number of non zero entries nnz (right) against the L^2 error; $h = 0.75a/2$ and $ka = 10\pi$.

In the same manner, numerical experiments are carried out for the wavenumber $ka = 15\pi$. Results of Figure 10 exhibit similar trends for the convergence rate and conditioning. Compared with the previous case (Figure 9(a)), the results show a decrease of the condition number by two orders of magnitude in the asymptotic region. In fact, this was expected as the condition number decreases with the wavenumber. Again, a notable saving in the number of non zero entries is also achieved in the global matrix of BBFEMs. In contrast to PUFEM, the ill-conditioning issue related to static condensation with a high polynomial order restricts the use of BBFEMs for tackling wave problems with multi-wavelength sized elements, where a further increase of the polynomial order is needed to improve the wave resolution.

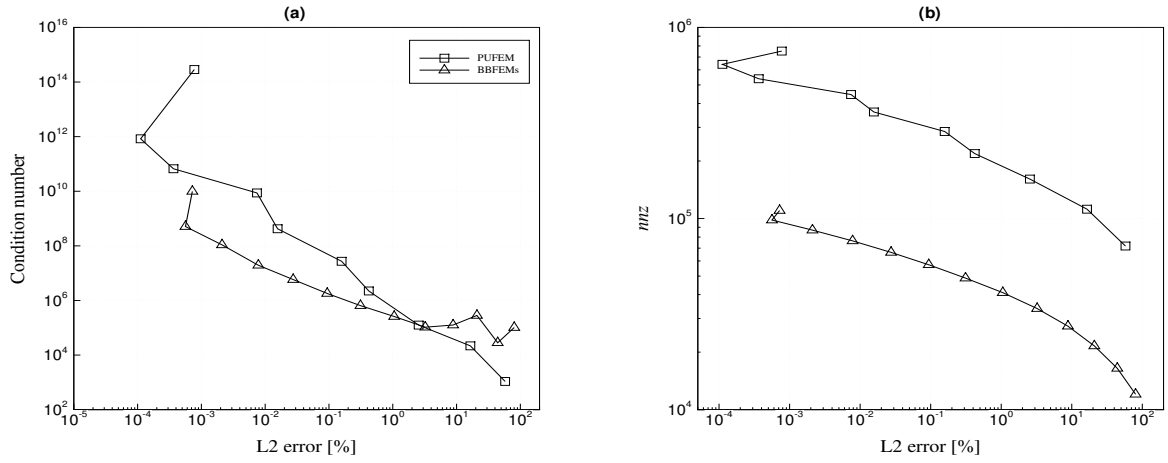

Figure 10: The condition number (left) and number of non zero entries nnz (right) against the L^2 error, for a mesh size $h = 0.75a/2$; $ka = 15\pi$.

5.3.2 Convergence and conditioning analysis: h-refinement

The approach adopted in this study is inspired from [9]. BBFEMs is compared against PUFEM, for

fixed polynomial orders and numbers of enriching plane waves by varying the mesh resolution, for the wavenumbers $ka = 25\pi$ and $ka = 50\pi$, where the pollution error may affect the accuracy. The numerical experiments are performed on the sequence of mesh grids from M_1 to M_f (see Figure 4). The L^2 error and condition number are plotted against the number τ_λ of DoF per wavelength, in Figure 11, for the wavenumber $ka = 25\pi$. The polynomial order p and number m of enriching plane waves are indicated on each curve. As expected, both methods lead to a low number of DoF per wavelength as the polynomial order or the number of plane waves increase. For instance, to achieve an engineering accuracy of around 1%, using PUFEM, it is better to use a relatively coarse mesh and take a large number of plane waves, $m = 12$, which leads to $\tau_\lambda \backsimeq 4$, while a finer mesh grid with a low number of plane waves, $m = 4$, requires $\tau_\lambda \backsimeq 8$. However, BBFEMs requires only $\tau_\lambda \backsimeq 2$ with a polynomial order $p = 12$ (see Figure 11(a)). It is also observed from Figure 11(a) that BBFEMs enters the asymptotic regime with a low number of DoF per wavelength and has a better algebraical decay rate compared to that of PUFEM. A fast increase of the condition number of PUFEM with respect to the number of DoF per wavelength is observed in Figure 11(b), while it remains below an upper bound with BBFEMs. The effect of ill-conditioning on the accuracy of PUFEM is also seen with a further increase of both grid resolution and number of plane waves. This problem is commonly known in PUFEM to be related to the use of a large number of enriching wave functions on small size elements compared to the wavelength [56]. However, the conditioning of PUFEM when the wave is not sufficiently well resolved is better. It is worth noticing that with a poor grid resolution, resonant frequencies may affect the conditioning of the bubble matrices $\boldsymbol{B}_e$ and consequently it also affects the conditioning of the condensed global matrix.

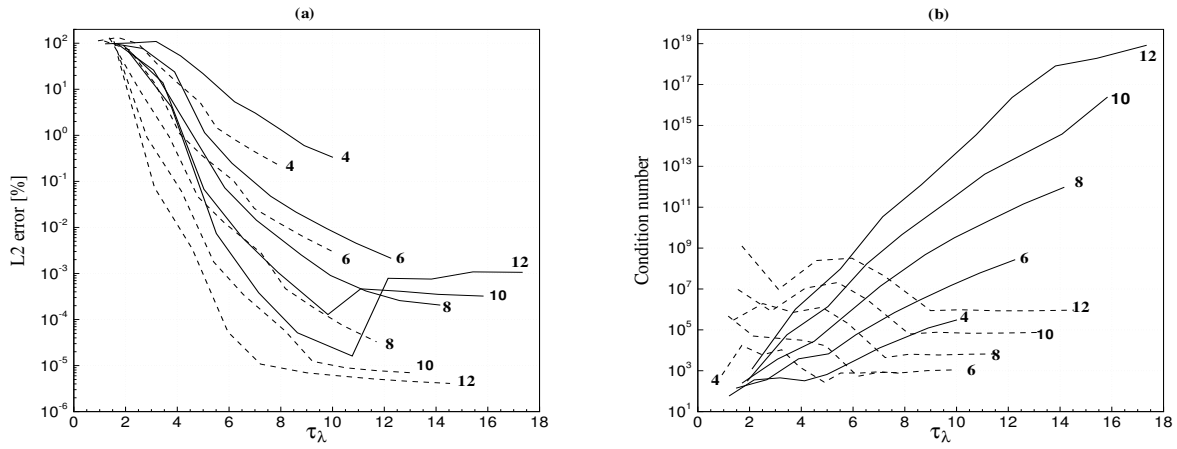

Figure 11: The L^2 error (left) and condition number (right) against τ_λ; $ka = 25\pi$. Solid lines (PUFEM), dashed lines (BBFEMs).

Results for the wavenumber $ka = 50\pi$ are illustrated in Figure 12. They show a similar trend of the L_2 error decay with respect to τ_λ to that seen for the case of $ka = 25\pi$ (see Figure 12(a)). Moreover, a decrease of the condition number of both schemes with the wavenumber ka is clearly observed in Figure 12(b), compared to the results of Figure 11(b). Unless a high accuracy solution is sought, the conditioning of PUFEM is clearly better. Similar observations were made in [9], with high order Lobatto polynomials and wave based methods.

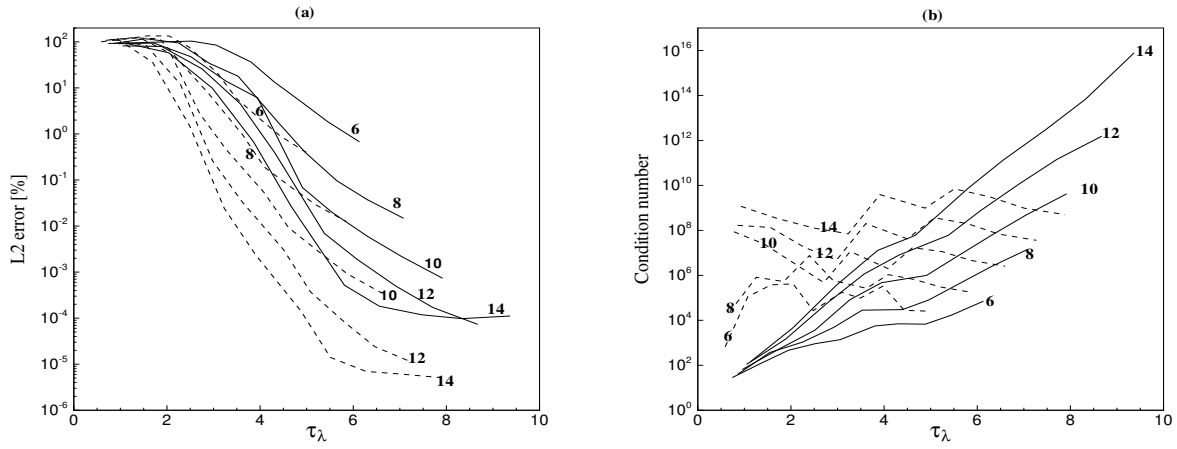

Figure 12: The L^2 error (left) and condition number (right) against τ_λ; $ka = 50\pi$. Solid lines (PUFEM), dashed lines (BBFEMs).

Here the performance of PUFEM and BBFEMs in term of memory requirements is further examined. Figure 13 shows the required factorisation memory in MBytes to achieve a prescribed accuracy, for different polynomial orders. For the sake of clarity, results corresponding to $m = p = 6$ are not included. It is obvious that high order methods require less memory than low order ones to achieve a given accuracy. Moreover, compared to PUFEM, BBFEMs yields significant saving in term of factorisation memory.

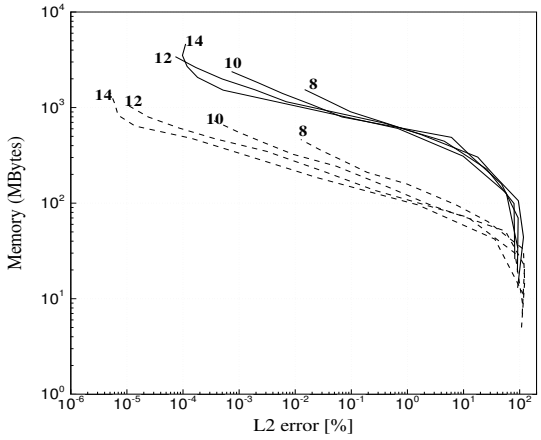

Figure 13: Factorisation memory versus the L^2 error. Solid lines: PUFEM; dashed lines: BBFEMs

5.4 Wave scattering by a rigid cylinder

The numerical experiments in this benchmark problem are performed on the same sequence of gradually refined mesh grids depicted in Figure 4. Once again, BBFEMs is assessed against PUFEM, in the same way followed in Subsection 5.3.2, with the wavenumbers $ka = 25\pi$ and $ka = 50\pi$. For these values of ka about of $N_t = 87$ and $N_t = 175$ modes are included, respectively, in the wave scattering analytical solutions. Figures 14 and 15 show the L^2 error and condition number versus

the number τ_λ of DoF per wavelength. Similar trends of the L^2 error decay and condition number increase with respect to τ_λ can be observed, compared to the results of the previous benchmark problem, and the overall conclusions are:

- The L^2 error decay of BBFEMs is better compared to that of PUFEM.
- PUFEM yields a low condition number with a poor grid resolution.
- For a well resolved solution, the conditioning of BBFEMs stays acceptable, while that of PUFEM grows significantly.

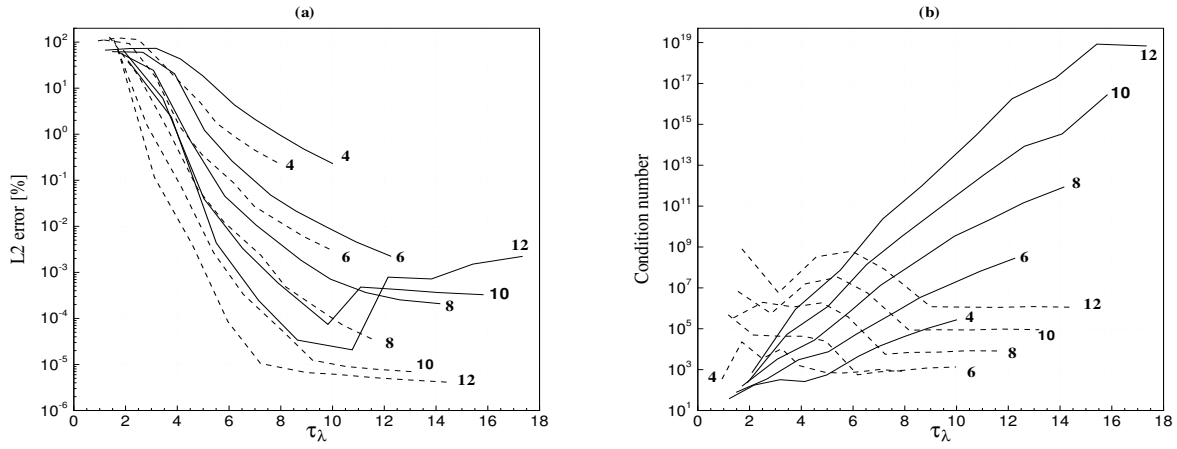

Figure 14: The L^2 error (left) and condition number (right) against τ_λ; $ka = 25\pi$. Solid lines: PUFEM; dashed lines: BBFEMs

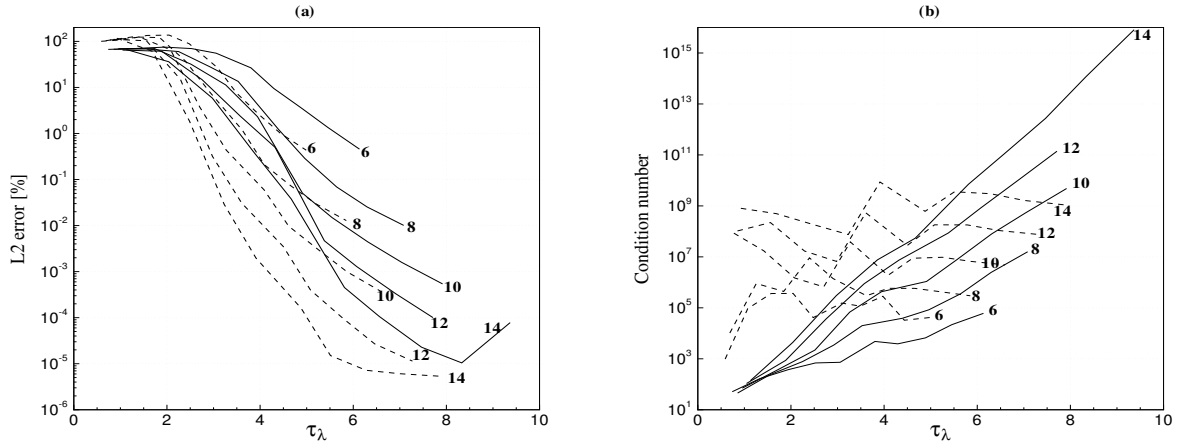

Figure 15: The L^2 error (left) and condition number (right) against τ_λ; $ka = 50\pi$. Solid lines: PUFEM; dashed lines: BBFEMs

5.5 L-shaped domain problem

The problem of wave scattering at corners has been dealt with by several authors. Its solution presents a singularity and the proposed solution models have been enriched by fractional order Bessel functions emanating from the corners [59–62].

The numerical experiments in this test problem are performed on the four mesh grids depicted in Figure 5. First, results using a uniform q-refinement are presented. It is worth noticing that the number τ_λ of DoF per wavelength cannot be used as an indicator for this benchmark test, as the mesh grid is not quasi-uniform. Figure 16 shows the L^2 error and condition number against the number nnz of non zero entries in the global matrix, for the wavenumber $ka = 10\pi$. It is observed from Figure 16(a) that with both methods the fast decay of the L^2 error is lost. Moreover, the accuracy of the two schemes cannot be further enhanced with a low grid resolution around the corner, even if the polynomial order or the number of enriching plane waves are increased. This behaviour is expected for problems with non-smooth solutions, where the error due to the singularity predominates the overall numerical error (see [38,51]). It is also observed that the accuracy of both methods improves by a local h-refinement around the corner, but an adaptive choice of the number of enriching wave functions is needed within PUFEM to avoid the high level of conditioning (see Figure 16(a)) related to the use of a large number of plane waves on small size elements, compared to the wavelength.

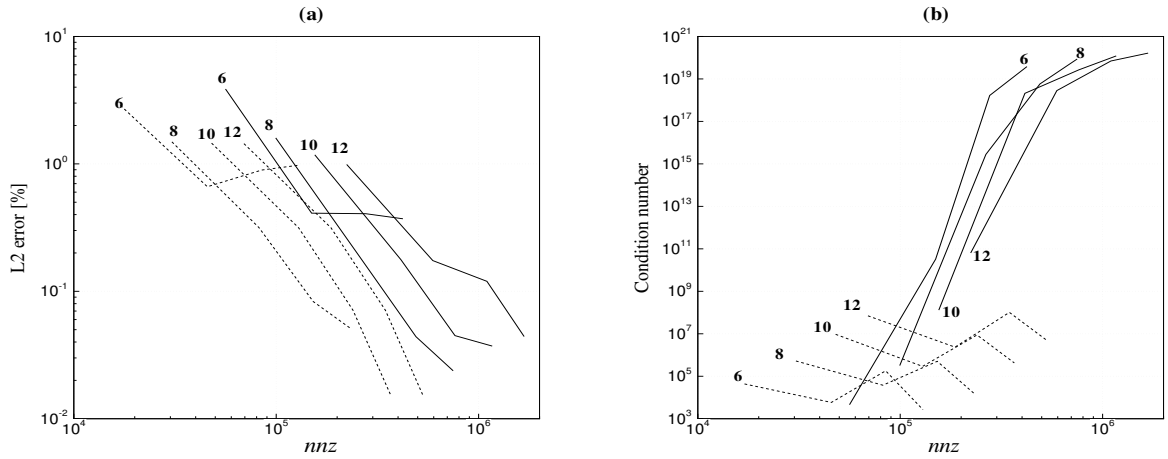

Figure 16: The L^2 error (left) and condition number (right) versus the number of non zero entries nnz in the global matrix; $k = 10\pi$. Solid lines: PUFEM; dashed lines: BBFEMs

Now, numerical results using a non uniform q-refinement are given. The adopted approach here is based on *a priori* information indicator, which is the local wave resolution defined by

$$r_{T_e} = \frac{h_{T_e}}{\lambda q_{T_e}}, \tag{29}$$

where h_{T_e} is an element mesh size and q_{T_e} refers to the largest polynomial order or the number of plane waves attached to a triangular element T_e. Initially, a fixed refinement parameter $q^0_{T_e}$ is chosen. In the finer region of the mesh grid, where the preasymptotic condition

$$\frac{h_{T_e}}{\lambda} \leq \frac{1}{10} \tag{30}$$

holds, the number q_{T_e} is set equal to 2. This means that the element mesh size h_{T_e} is at least one order of magnitude smaller than the wavelength λ. When PUFEM is adopted, the carried out numerical experiments indicate that for an element T_e such that $\frac{1}{10} < \frac{h_{T_e}}{\lambda} \leq 1$, the parameter q_{T_e} can be increased in a linear way from 2 to the value $q^0_{T_e}$ used in the coarse region, by keeping $r_{T_e} \simeq \frac{1}{20}$,

i.e. the same ratio of the preasymptotic condition. More precisely, in the region $\frac{n}{10} < \frac{h_{T_e}}{\lambda} \leq \frac{n+1}{10}$, with $1 \leq n \leq 9$, the parameter q_{T_e} is chosen such that

$$q_{T_e} = \frac{1}{r_{T_e}} \frac{h_{T_e}}{\lambda} \simeq 20 \times \frac{n}{10} = 2n. \tag{31}$$

In the case where the integer $n > \frac{q^0_{T_e}}{2}$, the rule (31) is not used and the parameter q_{T_e} is set equal to $q^0_{T_e}$. Let us point out that the polynomial order of BBFEMs still contributes in improving the overall error outside the preasymptotic region so that only the rule (30) is considered. Regarding conformity, it is automatically fulfilled for PUFEM and BBFEMs, as the polynomial order and number of enriching plane waves are attached to vertex and edge elements.
Comparison results for PUFEM in terms of the L_2 error and condition number against the number nnz of non zero entries are shown in Figure 17, for the wavenumber $ka = 20\pi$ with $q^0_{T_e} = 14$. In a similar way, comparison results for BBFEMs are depicted in Figure 18, where PUFEM(A) and BBFEMs(A) refer to the same schemes with a non uniform q-refinement.

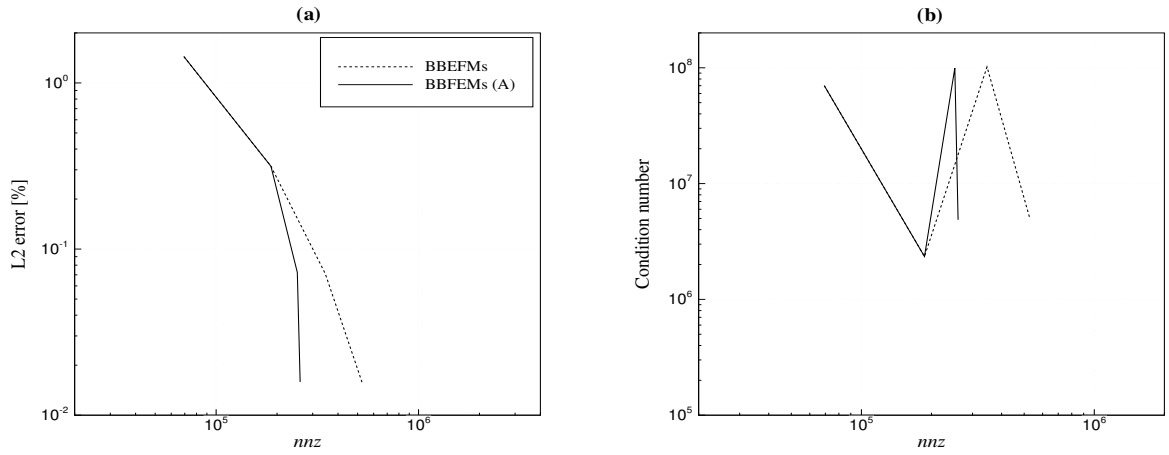

Figure 17: The L^2 error (left) and condition number (right) versus nnz; $k = 10\pi$. Solid lines: BBFEMs (uniform q-refinement); dashed lines: BBFEMs(A) (non uniform q-refinement, with $m = 14$)

The advantage of non uniform q-refinement for BBFEMs in reducing the total number of DoF is seen in Figure 17(a) and Figure 17(b), as the grid resolution around the corner is increased, while the accuracy and conditioning remain practically unchanged. Within PUFEM, in addition to the significant reduction of the total number of DoF, there is an improvement of both conditioning and accuracy as it can be seen in Figure 18(a) and Figure 18(b). A method to achieve a fast convergence rate for such adaptive procedures consists to use geometrically refined meshes, with an appropriate p-adaptivity [52–54].

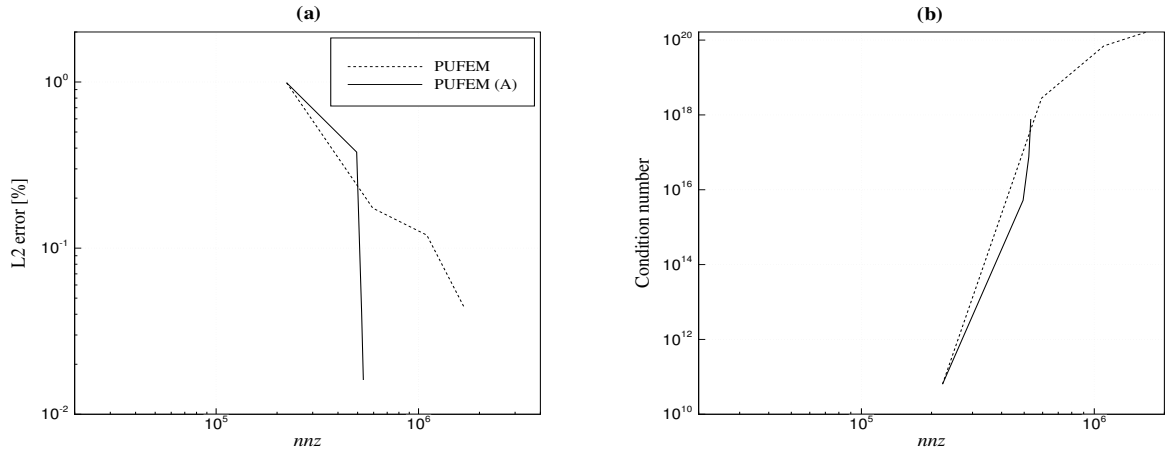

Figure 18: The L^2 error (left) and condition number (right) versus nnz: $k = 10\pi$. Solid lines: PUFEM (uniform p-refinement); dashed lines: PUFEM(A) (non uniform q-refinement, with $p = 14$)

Significant extra fill-in is observed, particularly when solving the L-shaped domain problem using PUFEM, on non quasi-uniform mesh containing small size elements, compared to the wavelength, around the re-entrant corner. This is examined for both methods and Table 1 shows the percentage p_f of fill-in for different mesh grids, computed from expression (24), for the wavenumber $ka = 20\pi$ with and without q-enrichment, and the number of plane waves $m = 14$. As the grid resolution increases around the corner, Table 1 indicates an increase of the extra fill-in by up to 10%. This issue which may lead to memory resources limitation problem, when using a direct sparse solver based on LU factorisation, is often characterised by a high level of conditioning as it is shown previously. Similarly, results obtained with BBFEMs, for the wavenumber $ka = 20\pi$ and polynomial order $p = 14$, are reported in Table 2. In contrast to PUFEM, the extra fill-in issue is not very pronounced when using BBFEMs, as it can be observed from Table 2.

	PUFEM				PUFEM (A)			
Mesh grids	n_{dof}	nnz	n_f	$p_f[\%]$	n_{dof}	nnz	n_f	$p_f[\%]$
M_1^L	4,046	303,177	688,513	4.28	4,046	303,177	688,513	4.28
M_2^L	10,402	807,723	3,388,470	3.15	10,129	770,552	3,144,931	3.08
M_3^L	19,026	1,494,507	19,611,104	5.44	13,307	901,599	4,373,165	2.48
M_4^L	28,910	2,281,881	80,948,557	9.71	14,853	927,986	4,805,137	2.18

Table 1: Percentage of fill-in in the global matrix before and after applying non uniform q-refinement for PUFEM; $m = 14$ and $ka = 20\pi$.

	BBFEMs				BBFEMs (A)			
Mesh grids	n_{dof}	nnz	n_f	$p_f[\%]$	n_{dof}	nnz	n_f	$p_f[\%]$
M_1^L	2,785	94,513	215,123	2.81	2,785	94,513	215,123	2.81
M_2^L	7,283	254,516	810,367	1.53	7,283	254,516	810,367	1.53
M_3^L	13,395	472,518	1,710,529	0.95	11,679	404,232	1,378,016	1.01
M_4^L	20,401	722,473	2,812,589	0.67	12,661	418,831	1,497,450	0.93

Table 2: Percentage of fill-in in the global matrix before and after applying non uniform q-refinement for BBFEMs; $p = 14$ and $ka = 20\pi$.

The benefit of using non uniform q-refinement is well illustrated based on a simple indicator. This motivates the investigation of efficient adaptive methods and/or *a posteriori* indicators, in order to provide an automatic choice of the polynomial order and elements mesh size for a given wavenumber, leading to a better accuracy with a reduced total number of DoF.

6 Conclusions

In this work, numerical aspects of BBFEM on unstructured triangular mesh grids are investigated. This high order scheme has been compared against PUFEM to assess its performance based on three benchmark problems. The key technique to obtain a good performance from BBFEM is the use of static condensation. A surprising outcome of this comparative study was that the conditioning of PUFEM was found to be acceptable and slightly better when the wave pattern is not well resolved. However, as the wave resolution increases the conditioning of PUFEM deteriorates. Furthermore, BBFEM with static condensation is able to provide good quality results. In general, it can be concluded that high order methods are more accurate and effective in coping with the pollution effect than low order methods. The results of benchmark tests have highlighted the benefit of BBFEM in reducing memory requirements and its flexibility in dealing with non-smooth problems by using local h-refinement. PUFEM, however, requires an adaptive approach to alleviate the ill-conditioning and extra fill-in issues.
An important question for future investigation is to determine an alternative FE formulation allowing numerical dissipation to enhance the stability of static condensation in order to allow a further increase of the polynomial order and hence tackle the case of multi-wavelength sized elements. It would also be useful to develop efficient adaptive methods and/or *a posteriori* indicators, such as those devised for FE Helmholtz problems in [10, 63], to render BBFEM more competitive for wave problems with varying and eventually discontinuous wavenumber, where non quasi-uniform mesh grids are needed. In 3D Helmholtz applications, it is expected to obtain similar trends when comparing PUFEM and BBFEMs in terms of conditioning and accuracy. Finally, it is worth noticing that there are closed form expressions for the evaluation of the mass and stiffness element matrices, involving Bernstein polynomials, over a simplex. In the presence of simplices with curved edges and/or variables coefficients, fast and efficient quadratures available in the literature [43, 44] can be used.

References

[1] F. Ihlenburg and I. Babuška. Finite-element solution of the Helmholtz-equation with high wavenumber. Part I: the h-version of the FEM. *Computers and Mathematics with Applications.* 1995; **30**: 9–37.

[2] F. Ihlenburg and I. Babuška. Finite element solution of the Helmholtz equation with high wavenumber. Part II: The h-p version of the FEM. *Siam Journal on Numerical Analysis.* 1997; **34**: 315–358.

[3] I. Babuška and S. A. Sauter. Is the pollution effect of the FEM avoidable for the Helmholtz equation considering high wave numbers? *SIAM Review.* 2000; **42**(3): 451–484.

[4] M. Ainsworth. Discrete dispersion relation for hp-version finite element approximation at high wave number. *SIAM J. Numer. Anal.* 2004; **42**(2): 553–575.

[5] M. Ainsworth. Dispersive and dissipative behaviour of high order discontinuous Galerkin finite element methods. *J. Comput. Phys.* 2004; **198**(1): 106–130.

[6] S. Petersen, D. Dreyer and V. O. Estorff. Assessment of finite and spectral element shape functions for efficient iterative simulations of interior acoustics. *Comput. Methods Appl. Mech. Eng.* 2006; **195**: (44–47) 6463–6478.

[7] G.W. Zumbusch. Symmetric hierarchical polynomials for the hp-version of finite elements. *Technical Report SC-93-32, Konrad-Zuse-Zentrum, Berlin, Germany.* 1993.

[8] J. M. Melenk. On condition numbers in hp-FEM with Gauss Lobatto-based shape functions. *J. Comput. Appl. Math.* 2002; **139**: 21–48.

[9] A. Lieu, G. Gabard and H. Bériot. A comparison of high-order polynomial and wave-based methods for Helmholtz problems. *Journal of Computational Physics.* 2016; **321**: 105–125.

[10] H. Bériot, A. Prinn and G. Gabard. Efficient implementation of high-order finite elements for Helmholtz problems. *Int. J. Numer. Meth. Eng.* 2015; **106**: 213–240.

[11] H. Bériot, G. Gabard and E. Perrey-Debain. Analysis of high-order finite elements for convected wave propagation. *Int. J. Numer. Meth. Eng.* 2013; **96**(11): 665–88.

[12] G. Giorgiani, D. Modesto, S. Fernndez-Méndez and A. Huerta. High-order continuous and discontinuous Galerkin methods for wave problems. *Int. J. for Num. Meth. in Fluids.* 2013; **73**: 883–903.

[13] A. Huerta, A. Angeloski, X. Roca and J. Peraire. Efficiency of high-order elements for continuous and discontinuous Galerkin methods. *Int. J. Numer. Meth. Eng.* 2013; **96**: 529–560.

[14] P. Monk and D. Q. Wang. A least-squares method for the helmholtz equation. *Comp. Meth. Appl. Mech. Eng.* 1999; **175**(1): 121–36.

[15] I. Babuška and J. M. Melenk. The partition of unity finite element method: Basic theory and applications. *Comp. Meth. Appl. Mech. Eng.* 1996; **139**: (1–4) 289–314.

[16] I. Babuška and J. M. Melenk. The Partition of Unity Method. *Int. Jour. Num. Meth. Eng.* 1997; **40**: 727–758.

[17] O. Laghrouche and P. Bettess. Short wave modeling using special finite elements. *J. Comput. Acoust.* 2000; **8**(01):189–210. .

[18] O. Laghrouche, P. Bettess, E. Perrey-Debain and J. Trevelyan. Wave interpolation finite elements for helmholtz problems with jumps in the wave speed. *Comp. Meth. Appl. Mech. Eng.* 2005; **194**(2): 367–81.

[19] O. Cessenat and B. Després. Application of an ultra weak variational formulation of elliptic PDEs to the two-dimensional Helmholtz problem. *SIAM J. Numer. Anal.* 1998; **35**(1):255–99.

[20] O. Cessenat and B. Després. Using plane waves as base functions for solving time harmonic equations with the ultra weak variational formulation. *J. Comput. Acoust.* 2003; **11**(02): 227–38.

[21] T. Strouboulis, I. Babuška and K. Copps. The design and analysis of the generalized finite element method. *Comp. Meth. Appl. Mech. Eng.* 2000; **181**(1): 43–69.

[22] T. Strouboulis, K. Copps and I. Babuska. The generalized finite element method: an example of its implementation and illustration of its performance. *Int. J. Numer. Meth. Eng.* 2000; **47**(8): 1401–17.

[23] C. Farhat, I. Harari and L. P. Franca. The discontinuous enrichment method. *Comp. Meth. Appl. Mech. Eng.* 2001; **190**(48): 6455–6479.

[24] R. Tezaur and C. Farhat. Three-dimensional discontinuous Galerkin elements with plane waves and lagrange multipliers for the solution of mid-frequency Helmholtz problems. *Int. J. Numer. Meth. Eng.* 2006; **66**(5): 796–815.

[25] A. Gillman, R. Djellouli and M. Amara. A mixed hybrid formulation based on oscillated finite element polynomials for solving helmholtz problems. *J. Comput. Appl. Math.* 2007; **204**(2): 515–25.

[26] M. Amara, H. Calandra, R. Dejllouli and M. Grigoroscuta-Strugaru. A stable discontinuous Galerkin-type method for solving efficiently helmholtz problems. *Computers & Structures.* 2012; **106**: 258–72.

[27] E. Perrey-Debain, O. Laghrouche, P. Bettess and J. Trevelyan. Plane-wave basis finite elements and boundary elements for three-dimensional wave scattering. *Philos. Trans. R. Soc. Lond. A: Math., Phys. Eng. Sci.* 2004; **362**(1816): 561–77.

[28] M. J. Peake, J. Trevelyan and G. Coates. Extended isogeometric boundary element method (XIBEM) for two-dimensional helmholtz problems. *Comp. Meth. Appl. Mech. Eng.* 2013; **259**: 93–102.

[29] H. Riou, P. Ladevèze and B. Sourcis. The multiscale VTCR approach applied to acoustics problems. *J. Comput. Acoust.* 2008; **16**: 487–505.

[30] G. Gabard, P. Gamallo and T. Huttunen. A comparison of wave-based discontinuous Galerkin, ultra-weak and least-square methods for wave problems. *Int. J. Numer. Meth. Eng.* 2011; **85**(3): 380–402.

[31] D. Wang, R. Tezaur, J. Toivanen and C. Farhat. Overview of the discontinuous enrichment method, the ultra-weak variational formulation, and the partition of unity method for acoustic scattering in the medium frequency regime and performance comparisons. *International Journal for Numerical Methods in Engineering.* 2012; **89**(4): 403–417.

[32] K. Christodoulou, O. Laghrouche, M.S. Mohamed and J. Trevelyan. High-order finite elements for the solution of Helmholtz problems. Computers & Structures. 2017; **191**: 129–139.

[33] O. Laghrouche, A. El Kacimi and J. Trevelyan. A comparison of NRBC for PUFEM in 2D exterior Helmholtz problems at high wave numbers.*J. of Comp. and App. Mathematics*. 2010; **234**: 1670–1677.

[34] D. Gilbarg and N.S. Trudinger. Elliptic partial differential equations of second order. *Springer-Verlag*, 1983.

[35] R. Leis. Boundary value problems in mathematical physics. *Teubner, Wiley* , 1989.

[36] M. J. Lai and L. L. Schumaker. Spline functions on triangulations. Vol. **110** of Encyclopedia of Mathematics and its Applications, *Cambridge University Press, Cambridge*, 2007.

[37] M. Ainsworth. Pyramid algorithms for Bernstein-Bézier finite elements of high non-uniform order in any dimension. *SIAM Journal on Scientific Computing*. 2014; **36**: 543–569.

[38] G. E. Karniadakis and S. J. Sherwin. Spectral/hp element methods for computational fluid dynamics, Numerical Mathematics and Scientific Computation. *Oxford University Press, New York*, 2005.

[39] P. Šolín, K. Segeth and I. Doležel. Higher-Order Finite Element Methods. *Chapman & Hall, New York*, 2003.

[40] J. M. Melenk. On generalized finite element methods. PhD Thesis, *University of Maryland*, 1995.

[41] A. El Kacimi and O. Laghrouche. Improvement of PUFEM for the numerical solution of high frequency elastic wave scattering on unstructured triangular mesh grids. *International Journal for Numerical Methods in Engineering*. 2010; **84**: 330–350.

[42] R. C. Kirby. Fast simplicial finite element algorithms using Bernstein polynomials. *Numerische Mathematik*. 2011; **117**: 631–652.

[43] R. C. Kirby and K. T. Thinh. Fast simplicial quadrature–based finite element operators using Bernstein polynomials. *Numerische Mathematik*. 2012; **121**(2): 261–279.

[44] M. Ainsworth, G. Andriamaro and O. Davydov. Bernstein-Bézier Finite Elements of Arbitrary Order and Optimal Assembly Procedures. *SIAM Journal on Scientific Computing*. 2011; **33**: 3087–3109.

[45] M. Ainsworth, O. Davydov and L. L. Schumaker. Bernstein-Bézier finite elements on tetrahedral-hexahedral-pyramidal partitions. *Computer Methods in Applied Mechanics and Engineering.* 2016; **304**: 140–170.

[46] P. Bettess and J. Bettess. A profile matrix solver with built-in constraint facility. *Eng. Comput.* 1986; **3**: 209–216 .

[47] P. Grisvard. Elliptic problems in non-smooth domains. Vol. 24 of Monographs and Studies in Mathematics, *Pitman, Boston*, 1985.

[48] P. R. Amestoy, I. S. Duff and J. Y. L'Excellent. Multifrontal parallel distributed symmetric and unsymmetric solvers. *Computer Methods in Applied Mechanics and Engineering.* 2000; **184**(2–4): 501–520.

[49] G. Karypis and V. Kumar. METIS–A Software Package for Partitioning Unstructured Graphs, Partitioning Meshes, and Computing Fill-Reducing Orderings of Sparse Matrices Version 4.0. *University of Minnesota*, Sept. 1998.

[50] M. Arioli, J. Demmel and I. S. Duff. Solving sparse linear systems with sparse backward error. *SIAM Journal on Matrix Analysis and Applications.* 1989; **10**(2): 165–190.

[51] I. Babuška, B. Andersson, B. Guo, J.M. Melenk and H.S. Oh. Finite element method for solving problems with singular solutions. *J. Comput. Appl. Math.* 1996; **74** (1–2): 51–70.

[52] I. Babuška, W. Gui. The h, p and hp Versions of the Finite Element Method in 1 Dimension. Part I. The Error Analysis of the p-Version. *Numerische Mathematik.* 1986; **49**: 577–612.

[53] W. Gui. Hierarchical elements, local mappings and the h-p version of the finite element method, Part I. *J. Comput. Math.* 1988; **6**: 54–68.

[54] W. Gui. Hierarchical elements, local mappings and the h-p version of the finite element method, Part II. *J. Comput. Math.* 1988; **6**:142–156.

[55] T. Huttunen, P. Gamallo and R. Astley. Comparison of two wave element methods for the Helmholtz problem. *Commun. Numer. Meth. Eng.* 2009; **25** (1): 35–52.

[56] O. Laghrouche, P. Bettess and R. Astley. Modelling of short wave diffraction problems using approximating systems of plane waves. *Int. J. Numer. Meth. Eng* . 2002; **54** (10): 1501–1533.

[57] F. Ihlenburg. Finite Element Analysis of Acoustic Scattering. *Springer-Verlag, New York*, 1998.

[58] G. Pólya and G. Szegő. Isoperimetric Inequalities in Mathematical Physics. *Princeton University Press, Princeton, New Jersey*, 1951.

[59] A. H. Barnett and T. Betcke. An exponentially convergent nonpolynomial finite element method for time-harmonic scattering from polygons. SIAM Journal on Scientific Computing. 2010 May 21; **32** (3):1417–41.

[60] K. Serkh and V. Rokhlin. On the solution of the Helmholtz equation on regions with corners. Proceedings of the National Academy of Sciences. 2016 Aug 16; **113**(33): 9171–6.

[61] T. Luostari, T. Huttunen and P. Monk. Improvements for the ultra weak variational formulation. International Journal for Numerical Methods in Engineering. 2013 May 11; **94** (6): 598–624.

[62] C.J. Gittelson, R. Hiptmair and I. Perugia. Plane wave discontinuous Galerkin methods: analysis of the h-version. *ESAIM: Mathematical Modelling and Numerical Analysis.* 2009 Mar; **43**(2): 297–331.

[63] Irimie S., Bouillard P. A residual a posteriori error estimator for the finite element solution of the Helmholtz equation. *Computer methods in applied mechanics and engineering.* 2001; **190** (31): 4027–4042.